


Graphene-WS₂ van der Waals Hybrid Heterostructure for Photodetector and Memory Device Applications

Sreemanta Mitra^{✉,*}, Saloni Kakkar, Tanweer Ahmed^{✉,†} and Arindam Ghosh[‡]
Department of Physics, Indian Institute of Science, Bangalore 560012, India

 (Received 11 June 2020; revised 30 September 2020; accepted 27 October 2020; published 9 December 2020)

The intriguing electronic properties of graphene and the strong light-matter interaction in layered transition-metal dichalcogenide (TMDC) make them a natural partner for hybrid devices, not only for optoelectronic device applications, but also to understand the conversion of light to electricity in this atomic scale prototype of a donor-acceptor complex. Here, we describe graphene-on-WS₂ binary heterostructure FET device, displaying gate-tunable persistent photoconductivity. Our time-dependent photovoltage relaxation experiments suggest that the charge-transfer time scale in this heterostructure is dependent on the input optical power, contrary to what is observed for the bare TMDC and is orders of magnitude slower than that observed for various other vdW hybrids. The optoelectronic responsivity of this device at low optical power is found to be as high as 10¹⁰ V/W, and thus shows the potential to be one of the most sensitive visible range photodetectors, while the gate tunability of the persistent photoconductivity can be utilized in the memory device applications. We identify that the photoresponse is the outcome of a photogating mechanism, due to the exciton dissociation under optical excitation, followed by the trapping of holes in WS₂ and subsequent electron transfer to graphene.

DOI: [10.1103/PhysRevApplied.14.064029](https://doi.org/10.1103/PhysRevApplied.14.064029)

I. INTRODUCTION

Miniaturized photodetectors [1–5] with strong optoelectronic response and high speed are of great interest for a vast number of applications where charge transfers play a crucial role in device application by controlling electron-hole recombination [6]. Two-dimensional materials, with the discovery of graphene [7] have attracted significant attention in this, due to their intriguing electronic and optical properties [7–16], especially at the monolayer limit, and the possibility to easily integrate them into a heterostructure. A pristine graphene-based field effect photodetector has intrinsically poor optical responsivity (approximately mA/W) due to the absence of an optical energy band gap (E_g) and small carrier lifetime [17], however, they display an ultrafast timescale of photoresponse. On the other hand, monolayers semiconducting transition-metal dichalcogenides (TMDCs) are direct band-gap semiconductor with strong light-matter interaction [18]. Although only TMDC-based photodetectors show higher

photoresponsivity [19–21] compared to graphene photodetectors, the intrinsically low charge-carrier mobility of TMDC makes them challenging to use in high-speed applications. The timescale of photoresponse in these detectors is limited by slow trapping or detrapping of the photo-carriers. A wide range of temporal response time from milliseconds to hundreds of seconds has been shown in previous TMDC photodetectors, all correlated inversely with their responsivity [19].

Recently, van der Waals (vdW) hybrids of TMDC and graphene have emerged as the prototype material for optoelectronic and photonic applications and revolutionized the field with an enormous high value of responsivity (approximately equal to 5×10^8 A/W) [22,23]. The combination of a large optical absorption coefficient of TMDC and high charge-carrier mobility of graphene makes graphene-TMDC hybrids suitable for a plethora of optoelectronic applications. Furthermore, the implementation of graphene-TMDC vertical heterostructures allows TMDC → graphene photocarrier transfer with approximately ps timescale [24]. While significant effort has been given to graphene and TMDC-based FET devices for optoelectronic applications and understanding, WS₂ as the photoactive material in a graphene-WS₂ hybrid phototransistor has not been discussed in detail.

Here, we explore the effect of electron-hole separation in graphene on a WS₂ binary heterostructure interface by time-dependant photovoltage relaxation experiments and

*sreemanta85@gmail.com

†Present address: Cambridge Graphene Centre, Engineering Department, University of Cambridge, Cambridge CB3 0FA, United Kingdom.

‡arindam@iisc.ac.in; Also at: Centre for Nano Science and Engineering, Indian Institute of Science, Bangalore 560012, India.

discuss its possibility in photodetector and memory device applications. Our experiments reveal that the change of resistance of the channel material, to a slowly relaxing state under the photoexcitation, and this changed state persists even after switching off the excitation source, showing persistent photoconductivity. The emergence of persistent photoconductivity, and its tailoring by the gate voltage allowed its possibility as an optoelectronic memory device. Furthermore, the tunability of the magnitude of photoreponse and the charge-transfer process by the electrostatic gating also provide the platform for a graphene-based photodetector with superior responsivity. The details are reported here.

II. EXPERIMENT

A graphene-WS₂ binary vdW heterostructure is created by layer-by-layer dry transfer [25] of mechanically exfoliated graphene and WS₂ flakes to form vertical heterostructure and then transferred onto a SiO₂/Si⁺⁺ substrate, where the heavily doped *p*-type Si⁺⁺ acts as a global back gate. The device electrical contacts are defined by *e*-beam lithography and made by subsequent metalization of Cr(5 nm)/Au(50 nm). The device is primarily characterized using the Raman spectra [26–28].

In Fig. 1(a), we show the typical device architecture schematic and the measurement scheme. The WS₂ is covered with graphene, which acts as the measurement channel. The optical image of the graphene-WS₂ device (dev A) along with the electrical contacts is shown in Fig. 1(b). A similar device (dev B) with a bottom hexagonal boron nitride (*h*-BN) is also studied [Fig. 1(c)] to check the effects of the substrate on the observed phenomena. The graphene on WS₂, is outlined in both Figs. 1(b) and 1(c). We take a current-biased two-probe ac measurement technique for the measurements. A constant current (100 nA, with frequency approximately equal to 217 Hz) is applied to the device channel and the corresponding voltage is measured using a lock in (time constant = 30 ms) under optical illumination [Yellow light-emitting diode (LED), 590 nm, 2.10 eV] at low temperature (*T*) [22,29]. The measurement set up is described elsewhere [29].

III. RESULTS AND DISCUSSIONS

In Fig. 1(d), we show the PL of the graphene-WS₂ hybrid device at 300 K. The excitonic peak of WS₂ [30–33] is observed at 1.946 eV with a line-width of 144 meV as evident from the Lorentzian fit (black solid line) to the experimental data. The broadening is higher than the typical linewidth of a similarly thick WS₂ layer [30–32,34]. The sharp feature originated at around 2 eV arises due to the 2D Raman feature of graphene [26,35].

We begin to describe our transport data by showing the source-drain resistance (*R*) of the graphene channel as a function of back-gate voltage (*V*_{BG}) [Fig. 1(e)] for dev A in the dark state to understand its doping profile. We

observe the typical “bell-shaped” transfer characteristics of graphene on an insulating substrate. The charge neutrality point (Dirac point, *V*_{*D*}) for dev A, comes out to be -2.25 V, where *R* become maximum. For *V*_{BG} < *V*_{*D*}, the graphene is hole doped, while *V*_{BG} > *V*_{*D*} indicates conduction by electron. The hole and electron mobility in dev A is calculated to be 0.39 m²/Vs and 0.51 m²/Vs, respectively. The conduction threshold for the WS₂, appears at 15 V [36]. For *V*_{BG} > 15 V, WS₂ starts conducting and screens the *V*_{BG}, leading to a saturation of *R*. A similar transfer characteristic is observed for dev B, with a charge neutrality point at 2.85 V [Fig. 1(f)]. The number density in graphene is calculated using the scheme described in Refs. [22,37–39].

Figure 2(a) shows the transfer characteristic of dev A without (*R*_{dark}, in gray) and with (*R*_{light}, in red) the optical illumination, measured at 87 K. A positive (*R*_{light} > *R*_{dark}) and a negative (*R*_{light} < *R*_{dark}) photoresistance are observed in the hole- (*V*_{BG} < *V*_{*D*}) and the electron- (*V*_{BG} > *V*_{*D*}) doped regime. Due to the large optical transmission coefficient (approximately 98% [40]) of graphene and absorption coefficient of ten-layered WS₂ (approximately 30% [41,42]), excitons in WS₂ are dissociated under the optical illumination with photon energy (*E*_λ) greater than the excitonic energy (*E*_X) of WS₂. On either sides of graphene’s charge neutrality point, the transport is governed by holes or electrons as the majority carrier [7]. The photoexcited electrons from dissociated excitons of WS₂ are transferred to graphene and either recombine with the graphene’s holes or increase the number of electrons in graphene and thus provide either positive or negative photoresistance, respectively, and tuned by the *V*_{BG}. In Fig. 2(b) we show the time dependence of *R* with optical illumination (590 nm, *P* = 156 fWμm⁻²) at *V*_{BG} = -14 V for dev A. As the optical illumination is turned on, *R* increases from its dark-state value (*R*_{off}) and attain a relatively higher value (*R*_{on}). We define the change of resistance (photoresistance) as $\Delta R_{\text{sat}} = R_{\text{on}} - R_{\text{off}}$. The time dependence of *R* – *R*_{off} at different *V*_{BG} at a fixed *P* (1597 fWμm⁻²) and *T* (87 K) is shown in Fig. 2(c). A similar response is observed for room temperature also [43]. Since *R*_{off} is *V*_{BG} dependent [Fig. 1(e)], *R* – *R*_{off} is normalized in Fig. 2(c). A strong *V*_{BG} dependence of ΔR_{sat} is observed. A similar nature is observed for dev B [inset of Fig. 2(e)]. Figures 2(d) and 2(e) show the *V*_{BG} dependence of ΔR_{sat} , along with the $dR/dV_{\text{BG}} - V_{\text{BG}}$ for dev A and dev B, respectively. In the inset of Fig. 2(e), the time-dependent photoresistance is shown for dev B at two different *V*_{BG}s. The positive (for -2 V) and negative (for 8 V) photoresistance is observed, implying the photogenerated electrons move to the graphene channel and impact its conductivity, depending on its doping profile as mentioned earlier.

The photoresponse in TMDC FETs may arise due to two dominant mechanisms, namely, photovoltaic and photoconductive mechanisms [17]. The strong dependence of ΔR_{sat} on *V*_{BG} and observed proportionality between ΔR_{sat}

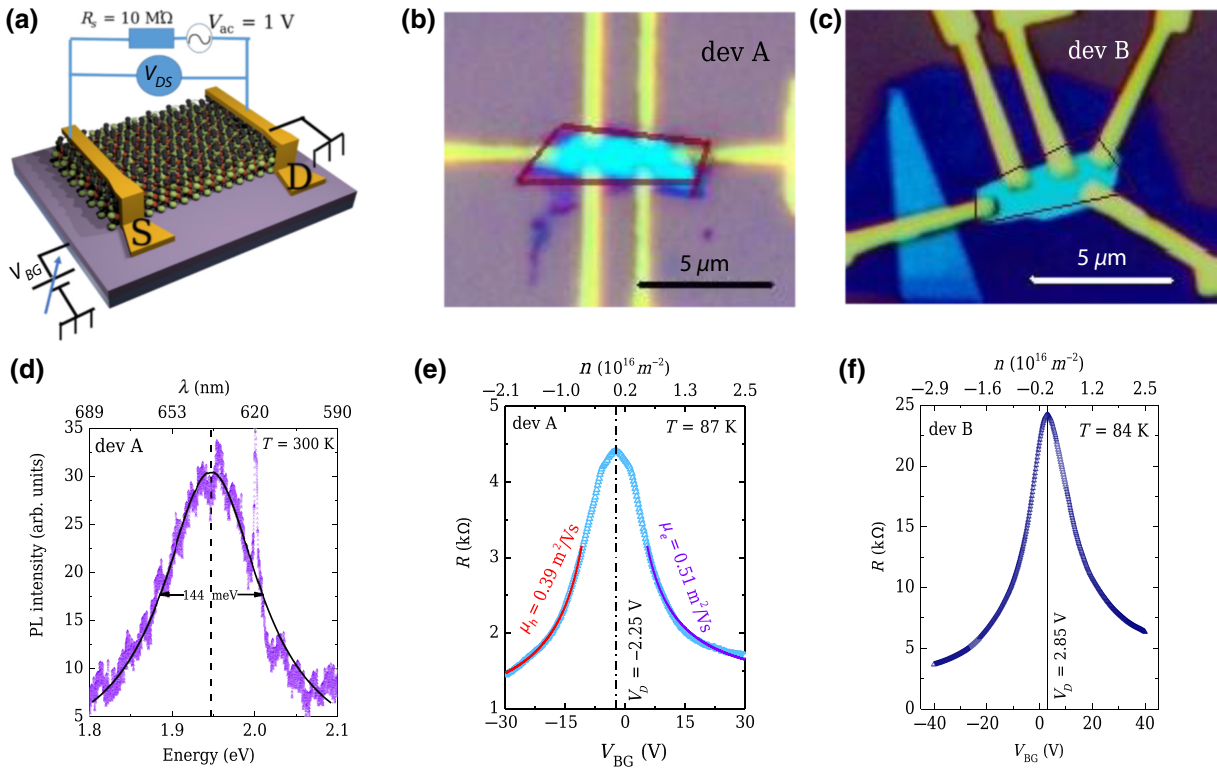


FIG. 1. Experimental consideration and primary characterizations. (a) Illustration of the graphene-WS₂ device architecture and electrical measurement set up. A constant current (100 nA) is applied between source (S) and drain (D) contact and the voltage drop (V_{DS}) is measured at low temperature under various optical illumination condition. The tunable dc gate voltage (V_{BG}) is applied to the p -doped Si⁺⁺. (b) Optical image of the graphene-WS₂ device (dev A). The graphene area is highlighted by the red line and it acts as the measurement channel. The scale is 5 μm . (c) Optical image of the graphene-WS₂/hBN device (dev B). The graphene area is highlighted by the red line. The h -BN thickness is 20 nm. The scale of the image is 5 μm . (d) PL spectra of dev A, measured at 300 K. Excitonic contribution from WS₂ is observed at 1.946 eV, with a linewidth of 144 meV. The black line is the Lorentzian fit to the experimental data. The sharp feature originated at around 2 eV arises due to the 2D Raman feature of graphene. (e) Transfer characteristics ($R - V_{BG}$) of dev A, measured at 87 K. The maximum of resistance (R) indicates the Dirac point (V_D) of dev A is -2.25 V. The solid lines are the fit to elucidate the electron and hole mobility of graphene as $0.51 \text{ m}^2/\text{Vs}$ and $0.39 \text{ m}^2/\text{Vs}$, respectively. (f) Transfer characteristics ($R - V_{BG}$) of dev B, measured at 84 K. The Dirac point (V_D) of dev B is 2.85 V. In both Figs. (e) and (f) the apparent independence of R at higher positive V_{BG} , indicates that WS₂ starts conducting around 15 V and screens the applied V_{BG} .

and dR/dV_{BG} in both of our devices, provide strong evidence of photogating effect, [17] in graphene-WS₂ vdW hybrids.

Figure 2(f) shows the photoresponsivity (γ , defined as the electrical output per optical input; V_P/P_{LED}) as a function of the V_{BG} , at a fixed optical power density, $1597 \text{ fW}\mu\text{m}^{-2}$. The value of photo responsivity increases with the increase in V_{BG} . At this optical power density the responsivity reaches an enormously large value of $2 \times 10^9 \text{ V/W}$.

Optical excitation of power density, P , creates an absorbed photon flux $\phi_a = \alpha P/E_\lambda$. α ($\approx 30\%$) is the absorption coefficient of ten-layered WS₂ [27,41,42] and $E_\lambda = hc/\lambda$ is the energy of a photon with wavelength λ , with h and c being Planck's constant and the speed of light in vacuum, respectively. The exciton population created by the ϕ_a is $n_x = \phi_a \tau_r$, where τ_r is the lifetime of radiative recombination [44]. At a given time t , the excited e can

transfer to graphene with probability $(N_G - n_G)/(N_G \tau_i)$. The τ_i , N_G , and n_G are the interlayer e transfer timescale, the total transferred e density at equilibrium and transferred e density at time t in graphene, respectively [45]. In this condition, the WS₂ \rightarrow graphene electron transfer process can be described by $dn_G/dt = n_x(N_G - n_G)/(N_G \tau_i)$, which leads to a transient change in the electron density in the graphene channel obeying, $n_G(t) = N_G[1 - e^{-(t-t_0)/\tau}]$ [44], where $\tau = (N_G/\phi_a)(\tau_i/\tau_r)$ is the timescale of devices' photoresponse and optical illumination is turned on at $t = t_0$.

At different values of V_{BG} , the exponential rise of N_G leads to the observed exponential change in R , following,

$$R(t) = R_{\text{off}} + \Delta R_{\text{sat}}(1 - \exp\{[-(t - t_0)/\tau]\}). \quad (1)$$

The persistent photoresistance after the illumination is turned off, can be a result of residual trapped holes in the

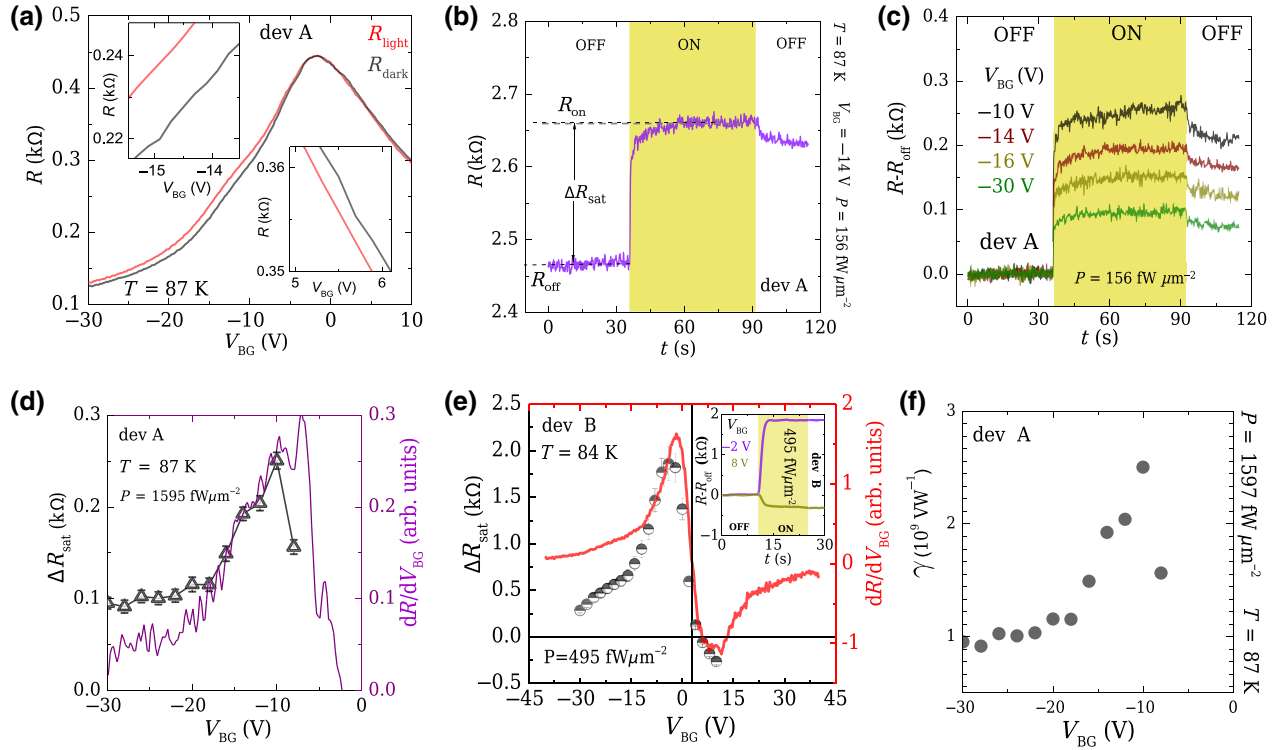


FIG. 2. Gate voltage dependence of the photoresponse. (a) The plots of source drain resistance (R) with the back gate voltage (V_{BG}) in the absence (grey) and presence (red) of light for dev-A. (Inset:) The magnified section of V_{DS} - V_{BG} curves at either sides of V_D ; left: $V_{BG} < V_D$, right: $V_{BG} > V_D$. (b) Change of R for a 60 s optical pulse ($\lambda_{ex} = 590$ nm or $E_\lambda = 2.1$ eV) at illumination power density $P = 156.5$ fW/ μm^2 in the hole doped regime ($V_{BG} = -14$ V) indicates the transfer of electrons to graphene from WS₂. R_{off} is the off-state (dark state) R , R_{on} is the steady-state R and ΔR_{sat} is the difference between R_{off} and R_{on} . (c) Plots of evolution of the photo resistance (or photo generated charge carrier accumulation magnitude for dev-A) in graphene for different V_{BG} . (d) Plots of V_{BG} dependence of photo response (ΔR_{sat}) along with the derivative of R - V_{BG} [see Fig. 1(e)]. The apparent proportionality of both the plots establishes the photogating mechanism. (e) The photogating mechanism for dev-B. (Inset:) Variation of R (normalized to the dark state value) at two different V_{BG} s for dev-B, measured for $P = 495$ fW/ μm^2 at $T = 84$ K. A positive photoresistance is seen for hole doped region while a negative photoresistance is seen for the electron doped region. (f) Variation of the responsivity with the V_{BG} for $P = 1597$ fW/ μm^2 measured at $T = 87$ K.

WS₂ layer [22]. Interestingly, τ can be tuned over 2 orders of magnitude by changing P . $R - R_{off}$ vs t at two different values of P are presented in Fig. 3(a). The solid lines are the fit to the experimental data using Eq. (1), resulting in $\tau = 2.8$ s and 33 s at two different P values, viz.; 156.5 and 0.6 fW/ μm^2 , respectively. The relaxation rate (τ^{-1}) varies linearly with P in a log-log plot, implying a power-law behavior [Fig. 3(b)]. The apparent proportionality of τ^{-1} and $P^{0.8}$ is consistent with $\tau^{-1} \propto \phi_a$. In the inset of Fig. 3(b), we show the variation of τ with P . At high P values, a saturation of τ^{-1} is observed, which is resulting from the limitation of measurement electronics.

The ΔR_{sat} (or photoresistance, PR) increases, as P increases, reaching approximately equal to 200 Ω for the highest power [Fig. 3(c)], leading to an 6% change. Contrary to the simple monolayer TMDC phototransistors, where PR almost decreases linearly with decreasing P [19,46], our hybrid FET devices, show a much slower

decrease of PR , i.e., it decreases by only a factor of 3 with a decrease of P by 4 orders of magnitude. This almost P -independent PR leads to an extremely high sensitivity (photoresponsivity, γ) in our graphene-WS₂ hybrid at low power, unlike the monolayer TMDC photodetectors [19,46]. We find that γ in this hybrid device reaches an extraordinary large value of approximately equal to 10^{10} V/W at P (approximately 1 fW/ μm^2) ($T = 87$ K) and decreases linearly as P is increased [Fig. 3(d)]. We attribute this high γ to the long carrier lifetime of photogenerated electrons in graphene along with their high mobility in graphene [22,47,48]. This makes our graphene-WS₂ hybrid suitable for extremely low-power applications such as night vision and space research.

To evaluate the device performance, we further calculate the photoconductive gain [49] as $G = \gamma hc/e\lambda$. It yields an enormous photo gain of 10^{10} . This large photoconductive gain arises due to the photogating effect, as a significantly

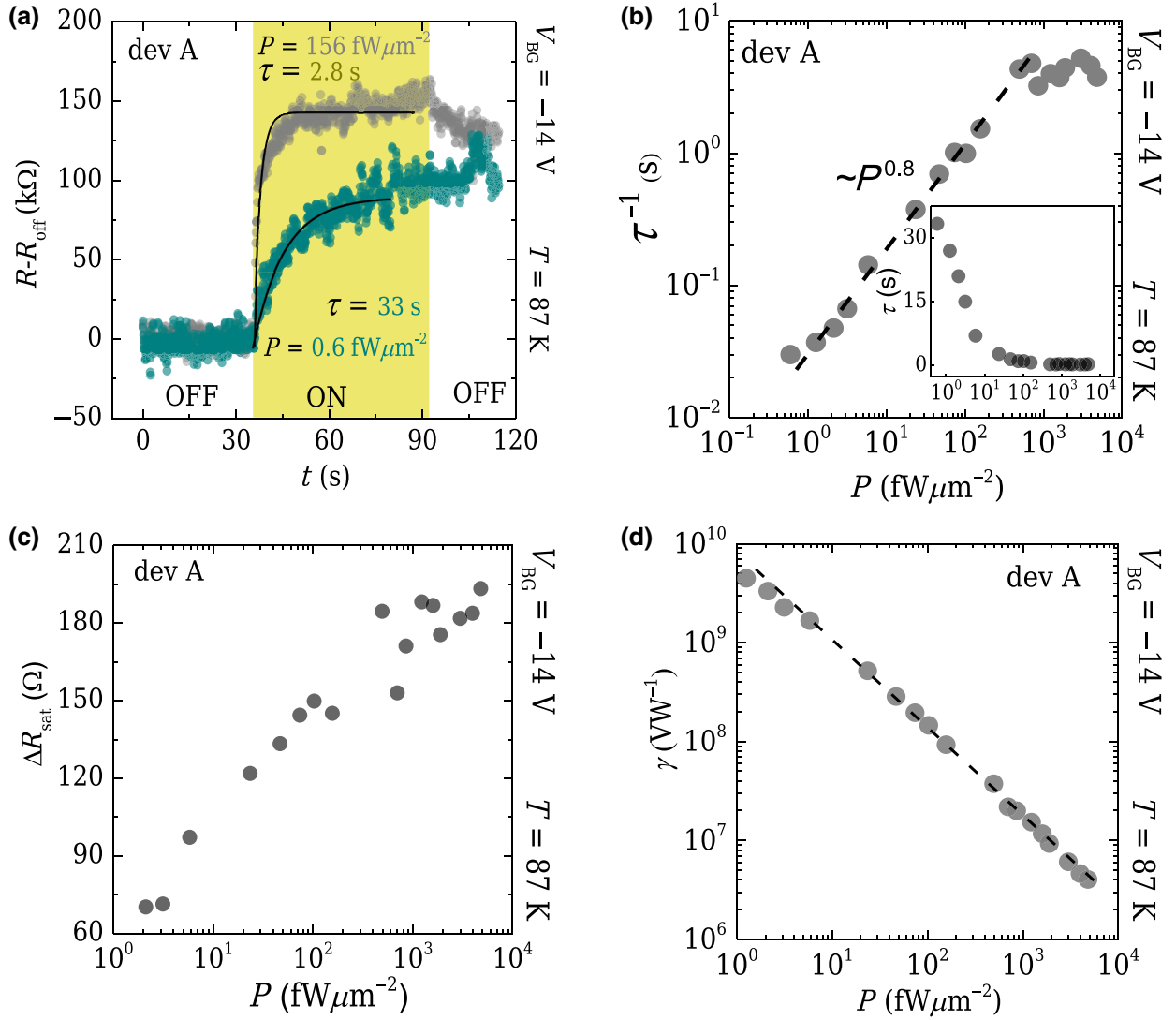


FIG. 3. Power dependence of the photoresponse for dev A, measured at 87 K. (a) Relaxation of R , for two different P , measured at $V_{BG} = -14$ V. The solid lines are fit to Eq. (1) to elucidate the relaxation time, τ . τ is found to increase as P is decreased. The numbers indicates the value of τ for the corresponding P . (b) The variation of relaxation rate (τ^{-1}) with P , for $V_{BG} = -14$ V. The linearity in the log-log representation, suggests a power-law dependence, with the exponent, 0.8. The dashed line is a fit to a generic power law behavior. (Inset) Power density (P) dependence of τ . (c) The plot of photoresistance (ΔR_{sat}) with P in a semilogarithmic representation. (d) Power dependence of the responsivity measured at $V_{BG} = -14$ V. The dashed line is the linear fit, suggesting γ follows $P^{-0.86}$. γ reaches to a substantially large value of 4×10^9 V/W at the lowest P .

large number of photoexcited carriers contribute to the photocurrent before recombining.

The steady-state electron density in graphene, N_G , is obtained from the optoelectronic response at different V_{BG} [Fig. 2(c)] and the transfer characteristics [Fig. 1(e)], using,

$$N_G = \frac{C \Delta R_{\text{sat}}}{e} / \frac{dR}{dV_{BG}} \quad (2)$$

N_G comes out to be approximately equal to 10^{15} m⁻² and is found to decrease as V_{BG} or $E_F (= \hbar v_F)$

$\sqrt{[C\pi(V_{BG} - V_D)]/e}$ is increased from the hole-doped regime to V_D [Fig. 4(c)]. For dev B, a similar value of N_G is observed [Fig. 4(d)], which follows the similar E_F dependence as dev A. From the experimentally observed $\tau = 200$ ms and $N_G = 10^{15}$ m⁻² at $V_{BG} = -14$ V and $P = 1597$ fW/μm² and considering $\tau_r \approx 10$ ps [44], the interlayer e transfer timescale can be estimated as $\tau_i = \tau \tau_r \phi_a / (N_G) \approx 1$ ns. This value is significantly larger than the previous experimentally reported τ_i in the graphene-TMDC hybrid [44], implying a relatively slower interlayer charge transfer across the graphene-WS₂ interface. The value of τ_i can depend on the relative alignment of the

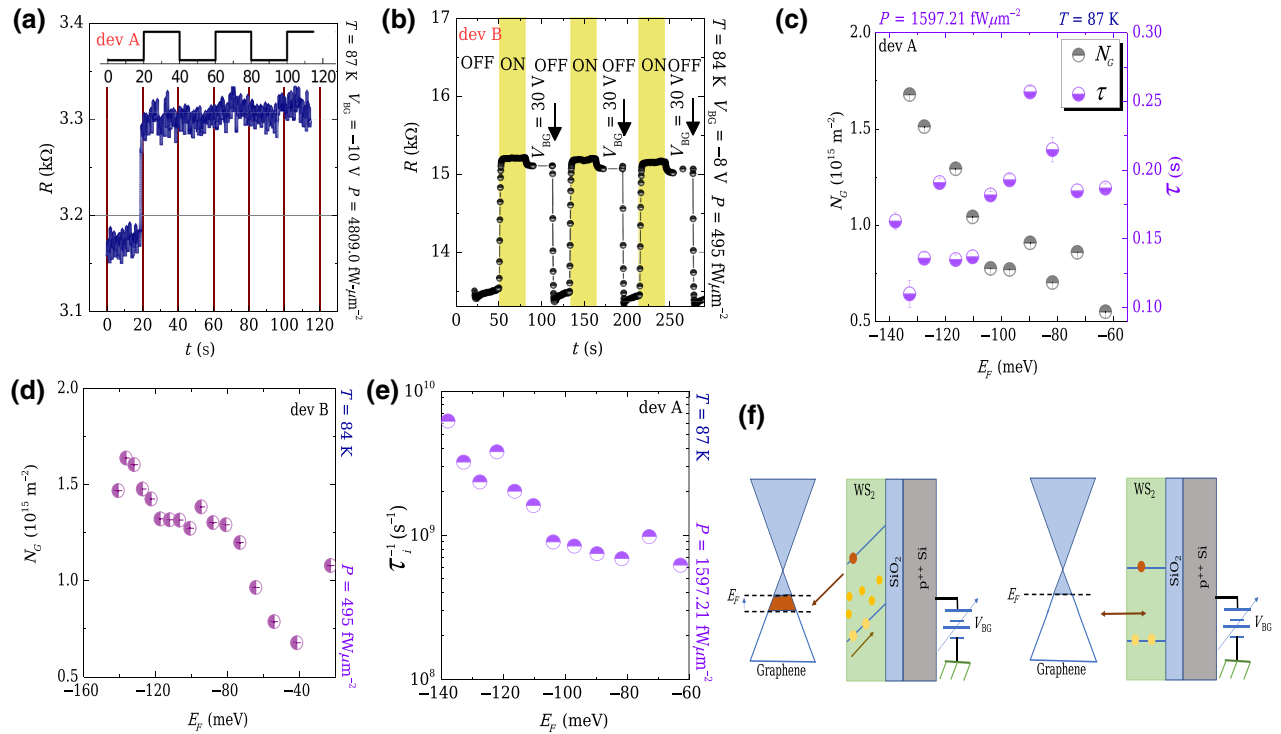


FIG. 4. Optical memory effect and charge-transfer mechanism. (a) Temporal dependence of R , under successive optical pulses measured at $V_{BG} = -10$ V and $P = 4809$ fW/ μm^2 , indicating near persistent photoconductivity in dev A. A similar persistence is observed for dev B. (b) The reset of the device (erasing memory) (measured for dev B). A $V_{BG} = 30$ V is applied to free the trapped holes by making WS_2 conducting and reset the device to its dark state. (c) Fermi energy (E_F) dependence of the steady-state charge-transfer magnitude (N_G) (left axis) and experimental time scale of charge transfer (τ) (right axis) measured for dev A. N_G is gradually decreasing with E_F increasing from the hole-doped region to the Dirac point, whereas, τ shows an increasing trend. (d) E_F dependence of N_G measured for dev B. The similar values of N_G suggests that the SiO_2 -TMDC interface has no significant effect in the observed persistent photoresistance observed in dev A or dev B and solely controlled by the trapped states in the WS_2 . (e) The E_F dependence of the calculated interlayer charge-transfer rate (τ_i^{-1}) for the graphene- WS_2 hybrid. τ_i^{-1} increases as E_F of graphene moves closer to the E_X of WS_2 . (f) Schematic of the charge-transfer process for $V_{BG} \ll V_T$ (left panel) and $V_{BG} \gg V_T$ (right panel). Red and yellow circles represent electrons and holes in the conduction and valence bands of WS_2 , respectively. The small black lines in the WS_2 is the trap states, which trapped the holes and electrons are subsequently transferred to the graphene.

Fermi energy (E_F) of graphene and the excitonic energy (E_X) in TMDC. In the case of the graphene- WS_2 hybrid, the excitonic state of WS_2 lies approximately equal to 400 meV below the Dirac point of graphene (considering undoped graphene's work function as 4.56 eV [50], electron affinity of WS_2 as 4.5 eV [51], and excitonic binding energy of WS_2 as approximately equal to 0.5 eV [52]). The observation of higher τ_i (slower charge transfer) can originate from the fact that $E_F > E_X$ for the graphene- WS_2 hybrid in our experimental regime.

The internal quantum efficiency [IQE = $\eta = (dn_G/dt)/\phi_a$; considering dn_G/dt at $t = t_0$, we get $\eta = N_G/\tau\phi_P$], [44] comes out to be approximately equal to 1%, which is consistent with previous reports for other graphene-TMDC-based devices [29].

In the case of TMDC-based photodetectors, photoresponse ceases when the illumination is turned off

[19,46]. However, in the case of this binary hybrid (both dev A and dev B), we observe that R continues to stay in the R_{on} value even after the light is turned off, attaining a persistence. Once it reaches the saturation state, it becomes practically insensitive to the subsequent optical pulses [Fig. 4(a)]. The physical separation between the photogenerated electrons and holes prevent these to recombine with each other, leading to this persistence with slow logarithmic relaxation. Although it is noted that the photodetection needs a faster response with no persistence, with the sufficiently long carrier lifetime, this persistent photoconductivity can lead to a memory device application. One of the ways to reset the device for next photodetection application is to apply large positive V_{BG} , making WS_2 conducting, and free the trapped holes [53]. In Fig. 4(b), we show that in the light-off condition, the application of a large V_{BG} erases the

persistence and takes the device (measured for dev B) back to its dark state. This process can be repeated several times without any effect on the responsivity or gain of the devices.

TMDC crystals are known to have intrinsic disorders in terms of crystallographic defects [54]. Extrinsic factors like residues and surface adsorbents appear during the fabrication process, and can lead to additional impurities in the TMDC FETS. Hole trapping by these impurities can create photogating effect due to an effective charge transfer [17]. Photogating effect arises due to the long-lived charge-trapping process, where the trapped charge at the TMDC-SiO₂ interface act as a gate through the capacitive coupling with the channel [17]. In a graphene-TMDC hybrid, photogating effect can happen when the photogenerated holes get stuck either at the traps in WS₂-SiO₂ interface, or at the bulk traps in WS₂. The trapped charges keep on accumulating, and act as a virtual gate. Alternatively, in this kind of hybrid device geometry, charge transfer can also lead to photogating, where the carrier density in graphene can be tuned by application of photons with energy greater than the band gap of the underlying semiconductor [44,45,47]. Similar trapping at the SiO₂-TMDC interface can also strongly impact photoresponse in graphene-WS₂ geometry. However, we observe N_G (approximately equal to 10^{15} m^{-2}) is orders of magnitude lower compared to the charge trap density [17] of thermally grown SiO₂ (approximately equal to 10^{19} m^{-2}). A similar value of N_G , is obtained for dev B, with *h*-BN as a substrate [Fig. 4(d)]. This implies that the trapping of charges at the SiO₂-WS₂ interface has no significant effect on the observed photoconductivity, and we attribute the observed photogating effect to the trapping of the holes in the bulk traps of WS₂ and subsequent *e* transfer to the graphene. In our graphene-WS₂ geometry we identify the WS₂ → graphene electron transfer, to be the primary source of observed photoresponse.

In Fig. 4(c), we show the E_F dependence of N_G , and the experimental time scale (τ) of photoresponse. It can be seen that N_G is decreasing as E_F of graphene is being shifted from the hole-doped regime towards the Dirac point, whereas, τ appears to increase. Based on these experimentally observed numbers, we calculate the E_F dependence of the interlayer charge-transfer rate ($\tau_i^{-1} = N_G/\tau\tau_r\phi_a$) [Fig. 4(e)]. As E_F of graphene is moved towards the excitonic level of WS₂, by the application of V_{BG} , τ_i^{-1} increases monotonically. A situation can not be disregarded for a possible resonance, where the charge-transfer rate becomes maximum, when E_F and E_X come to a same level. However, this requires further careful experiments at higher V_{BG} range. The mechanism of charge transfer and occurrence of the persistence in the hybrid is schematically shown in Fig. 4(f).

IV. SUMMARY

In summary, we discuss the gate tunable persistent photoconductivity in a graphene-on-WS₂ vdW hybrid FET device, with enormous responsivity and gain. We attribute this high performance to the combination of high carrier mobility in graphene. The mechanism of the photoreponse in the hybrid is identified to be the photogating due to the trapping of holes in the trapped states of WS₂ and subsequent electron transfer to the graphene. Our time-dependant photovoltage relaxation measurements further shows power-dependent experimental relaxation time of photoresponse, 10 to 12 orders of magnitude slower in this vdW hybrid than other vdW hybrids. The observed persistent photoconductivity is attributed to the trapping of photoexcited charges and is found to be tuned by the gate voltage. The ultrahigh responsivity and gate-tunable persistent photoconductivity makes the graphene-WS₂ hybrid a promising candidate for the visible range photodetector and memory device. The efficient photoconduction with astronomically high figure-of-merits of these devices at low optical power can find applications in miniaturized photodetectors to detect low intensity light and can be used in space science research, night vision, low light sensing camera etc. A natural extension of this superior responsivity at low optical power is to develop a single photon detector device for optical quantum-information applications. The optical memory effect, on the other hand, in these devices can find useful applications in removable mass storage media, virtual optical devices etc.

ACKNOWLEDGMENTS

S.M. thanks T. Phanindra Sai, Tathagata Paul, and Manjari Garg for various help and useful discussions. The authors thank CeNSE, IISc. for lithography support, optical and mechanical characterizations. The authors thank Department of Science and Technology (DST), India for the financial support.

-
- [1] V. W. Brar, M. C. Sherrott, and D. Jariwala, Emerging photonic architectures in two-dimensional opto-electronics, *Chem. Soc. Rev.* **47**, 6824 (2018).
 - [2] F. H. L. Koppens, T. Mueller, P. Avouris, A. C. Ferrari, M. S. Vitiello, and M. Polini, Photodetectors based on graphene, other two-dimensional materials and hybrid systems, *Nat. Nanotechnol.* **9**, 780 (2014).
 - [3] G. Konstantatos, Current status and technological prospect of photodetectors based on two-dimensional materials., *Nat. Commun.* **9**, 5266 (2018).
 - [4] Y.-F. Xiong, J.-H. Chen, Y.-Q. Lu, and F. Xu, Broadband optical-fiber-compatible photodetector based on a Graphene-MoS₂-WS₂ heterostructure with a synergetic photogenerating mechanism, *Adv. Electr. Mater.* **5**, 1800562 (2019).

- [5] W. Yu, S. Li, Y. Zhang, W. Ma, T. Sun, J. Yuan, K. Fu, and Q. Bao, Near-infrared photodetectors based on MoTe₂/Graphene heterostructure with high responsivity and flexibility, *Small* **13**, 1700268 (2017).
- [6] H. Wang, J. Bang, Y. Sun, L. Liang, D. West, V. Meunier, and S. Zhang, The role of collective motion in the ultrafast charge transfer in van der Waals heterostructures, *Nat. Commun.* **7**, 11504 (2016).
- [7] K. S. Novoselov, A. K. Geim, S. V. Morozov, D. Jiang, Y. Zhang, S. Dubonos, I. V. Grigorieva, and A. A. Firsov, Electric field effect in atomically thin carbon films, *Science* **306**, 666 (2004).
- [8] A. K. Geim and K. S. Novoselov, The rise of graphene, *Nat. Mat.* **6**, 183 (2007).
- [9] Z. Sun, A. Martinez, and F. Wang, Optical modulators with 2D layered materials, *Nat. Photon* **10**, 227 (2016).
- [10] R. Mas-Balleste, C. Gomez-Navarro, J. Gomez-Herrero, and F. Zamora, 2D materials: To graphene and beyond, *Nanoscale* **3**, 20 (2011).
- [11] M. Xu, T. Lian, M. Shi, and H. Chen, Graphene-like two dimensional materials, *Chem. Rev.* **113**, 3766 (2013).
- [12] S. Z. Butler *et al.*, Progress, challenges, and opportunities in two-dimensional materials beyond graphene, *ACS Nano* **7**, 2898 (2013).
- [13] J. A. Wilson and A. D. Yoffe, The transition metal dichalcogenides discussion and interpretation of observed optical, electrical, and structural properties, *Adv. Phys.* **18**, 193 (2006).
- [14] N. R. Pradhan, S. Talapatra, M. Terrones, P. M. Ajayan, and L. Balicas, Optoelectronic properties of heterostructures: The most recent developments based on graphene and transition-metal dichalcogenides, *IEEE Nanotechnol. Mag.* **11**, 18 (2017).
- [15] U. Wurstbauer, B. Miller, E. Parzinger, and A. W. Holleitner, Light–matter interaction in transition metal dichalcogenides and their heterostructures, *J. Phys. D: Appl. Phys.* **50**, 173001 (2017).
- [16] S. Mitra, D. Srivastava, S. S. Singha, S. Dutta, B. Satpati, M. Karppinen, A. Ghosh, and A. Singha, Tailoring phonon modes of few-layered MoS₂ by in-plane electric field, *npj 2D Mater. Appl.* **4**, 6 (2020).
- [17] M. M. Furchi, D. K. Polyushkin, A. Pospischil, and T. Mueller, Mechanisms of photoconductivity in atomically thin MoS₂, *Nano Lett.* **14**, 6165 (2014).
- [18] L. Britnell, R. M. Ribeiro, A. Eckmann, R. Jalil, B. D. Belle, A. Mishchenko, Y.-J. Kim, R. V. Gorbachev, T. Georgiou, S. V. Morozov, A. N. Grigorenko, A. K. Geim, C. Casiraghi, A. H. C. Neto, and K. S. Novoselov, Strong light-matter interactions in heterostructures of atomically thin films, *Science* **340**, 1311 (2013).
- [19] O. Lopez-Sanchez, D. Lembke, M. Kayci, A. Radenovic, and A. Kis, Ultrasensitive photodetectors based on monolayer MoS₂, *Nat. Nanotech.* **8**, 497 (2013).
- [20] W. Zhang, J.-K. Huang, C.-H. Chen, Y.-H. Chang, Y.-J. Cheng, and L.-J. Li, High-gain phototransistors based on a CVD MoS₂ monolayer, *Adv. Mater.* **25**, 3456 (2013).
- [21] W. Choi, M. Y. Cho, A. Konar, J. H. Lee, G.-B. Cha, S. C. Hong, S. Kim, J. Kim, D. Jena, J. Joo, and S. Kim, High-detectivity multilayer MoS₂ phototransistors with spectral response from ultraviolet to infrared, *Adv. Mater.* **24**, 5832 (2012).
- [22] K. Roy, M. Padmanabhan, S. Goswami, T. P. Sai, G. Ramalingam, S. Raghavan, and A. Ghosh, Graphene–MoS₂ hybrid structures for multifunctional photoresponsive memory devices, *Nat. Nanotech.* **8**, 826 (2013).
- [23] K. Roy, M. Padmanabhan, S. Goswami, T. P. Sai, S. Kaushal, and A. Ghosh, Optically active heterostructures of graphene and ultrathin MoS₂, *Solid State Commun.* **175**, 35 (2013), Special Issue: Graphene V: Recent Advances in Studies of Graphene and Graphene analogues.
- [24] M. Massicotte, P. Schmidt, F. Violla, K. G. Schädler, A. Reserbat-Plantey, K. Watanabe, T. Taniguchi, K. J. Tiel-rooij, and F. H. L. Koppens, Picosecond photoresponse in van der Waals heterostructures, *Nat. Nanotech.* **11**, 42 (2016).
- [25] S. Fan, Q. A. Vu, M. D. Tran, S. Adhikari, and Y. H. Lee, Transfer assembly for two-dimensional van der Waals heterostructures, *2D Mater.* **7**, 022005 (2020).
- [26] See Supplemental Material at <http://link.aps.org/supplemental/10.1103/PhysRevApplied.14.064029> for Raman spectroscopy of the devices.
- [27] A. Berkdemir, H. R. Gutiérrez, A. R. Botello-Méndez, N. Perea-López, A. L. Elías, C.-I. Chia, B. Wang, V. H. Crespi, F. López-Urías, J.-C. Charlier, H. Terrones, and M. Terrones, Identification of individual and few layers of WS₂ using Raman spectroscopy, *Sci. Rep.* **3**, 1755 (2013).
- [28] Y. Li, X. Li, T. Yu, G. Yang, H. Chen, C. Zhang, Q. Feng, J. Ma, W. Liu, H. Xu, Y. Liu, and X. Liu, Accurate identification of layer number for few-layer WS₂ and WSe₂ via spectroscopic study, *Nanotechnology* **29**, 124001 (2018).
- [29] K. Roy, T. Ahmed, H. Dubey, T. P. Sai, R. Kashid, S. Maliakal, K. Hsieh, S. Shamim, and A. Ghosh, Number-resolved single-photon detection with ultralow noise van der Waals hybrid, *Adv. Mater.* **30**, 1704412 (2018).
- [30] M. Currie, A. T. Hanbicki, G. Kioseoglou, and B. T. Jonker, Optical control of charged exciton states in tungsten disulfide, *Appl. Phys. Lett.* **106**, 201907 (2015).
- [31] W. Zhao, Z. Ghorannevis, L. Chu, M. Toh, C. Kloc, P.-H. Tan, and G. Eda, Evolution of electronic structure in atomically thin sheets of WS₂ and WSe₂, *ACS Nano* **7**, 791 (2013).
- [32] M. Currie, A. T. Hanbicki, G. Kioseoglou, and B. T. Jonker, Optical control of charged exciton states in tungsten disulfide, *App. Phys. Lett.* **106**, 201907 (2015).
- [33] T. S. Bhattacharya, S. Mitra, S. S. Singha, P. K. Mondal, and A. Singha, Tailoring light-matter interaction in WS₂–gold nanoparticles hybrid systems, *Phys. Rev. B* **100**, 235438 (2019).
- [34] See Supplemental Material at <http://link.aps.org/supplemental/10.1103/PhysRevApplied.14.064029> for PL spectroscopy of the similarly thick WS₂ flake used in fabricating the devices.
- [35] A. C. Ferrari, J. C. Meyer, V. Scardaci, C. Casiraghi, M. Lazzeri, F. Mauri, S. Piscanec, D. Jiang, K. S. Novoselov, S. Roth, and A. K. Geim, Raman Spectrum of Graphene and Graphene Layers, *Phys. Rev. Lett.* **97**, 187401 (2006).
- [36] D. Ovchinnikov, A. Allain, Y.-S. Huang, D. Dumcenco, and A. Kis, Electrical transport properties of single-layer WS₂, *ACS Nano* **8**, 8174 (2014).

- [37] See Supplemental Material at <http://link.aps.org/supplemental/10.1103/PhysRevApplied.14.064029> for calculation of number density in graphene.
- [38] A. Laturia, M. L. Van de put, and W. G. Vandenberghe, Dielectric properties of hexagonal boron nitride and transition metal dichalcogenides: from monolayer to bulk, *npj 2D Mater. Appl.* **2**, 6 (2018).
- [39] J. Guo, Y. Yoon, and Y. Ouyang, Gate electrostatics and quantum capacitance of graphene nanoribbons, *Nano Lett.* **7**, 1935 (2007).
- [40] R. R. Nair, P. Blake, A. N. Grigorenko, K. S. Novoselov, T. J. Booth, T. Stauber, N. M. R. Peres, and A. K. Geim, Fine structure constant defines visual transparency of graphene, *Science* **320**, 1308 (2008).
- [41] W. Zhao, R. M. Ribeiro, and G. Eda, Electronic structure and optical signatures of semiconducting transition metal dichalcogenide nanosheets, *Acc. Chem. Res.* **48**, 91 (2015).
- [42] C. E. Stevens, T. Stroucken, A. V. Stier, J. Paul, H. Zhang, P. Dey, S. A. Crooker, S. W. Koch, and D. Karauskaj, Super-radiant coupling effects in transition-metal dichalcogenides, *Optica* **5**, 749 (2018).
- [43] See Supplemental Material at <http://link.aps.org/supplemental/10.1103/PhysRevApplied.14.064029> for the room-temperature photoresponse of the device.
- [44] T. Ahmed, K. Roy, S. Kakkar, A. Pradhan, and A. Ghosh, Interplay of charge transfer and disorder in optoelectronic response in Graphene/hBN/MoS₂ van der Waals heterostructures, *2D Mater.* **7**, 025043 (2020).
- [45] R. Kashid, J. K. Mishra, A. Pradhan, T. Ahmed, S. Kakkar, P. Mundada, P. Deshpande, K. Roy, A. Ghosh, and A. Ghosh, Observation of inter-layer charge transmission resonance at optically excited graphene-TMDC interfaces, *APL Mater.* **8**, 091114 (2020).
- [46] Z. Yin, H. Li, H. Li, L. Jiang, Y. Shi, Y. Sun, G. Lu, Q. Zhang, X. Chen, and H. Zhang, Single-layer MoS₂ phototransistors, *ACS Nano* **6**, 74 (2012).
- [47] A. Pradhan, A. Roy, S. Tripathi, A. Som, D. Sarkar, J. K. Mishra, K. Roy, T. Pradeep, N. Ravishankar, and A. Ghosh, Ultra-high sensitivity infra-red detection and temperature effects in a graphene-tellurium nanowire binary hybrid, *Nanoscale* **9**, 9284 (2017).
- [48] S. Islam, J. K. Mishra, A. Kumar, D. Chatterjee, N. Ravishankar, and A. Ghosh, Ultra-sensitive graphene-bismuth telluride nano-wire hybrids for infrared detection, *Nanoscale* **11**, 1579 (2019).
- [49] C.-H. Yeh, H.-C. Chen, H.-C. Lin, Y.-C. Lin, Z.-Y. Liang, M.-Y. Chou, K. Suenaga, and P.-W. Chiu, Ultrafast monolayer In/Gr-WS₂-Gr hybrid photodetectors with high gain, *ACS Nano* **13**, 3269 (2019).
- [50] R. Yan, Q. Zhang, W. Li, I. Calizo, T. Shen, C. A. Richter, A. R. Hight-Walker, X. Liang, A. Seabaugh, D. Jena, H. Grace Xing, D. J. Gundlach, and N. V. Nguyen, Determination of graphene work function and graphene-insulator-semiconductor band alignment by internal photoemission spectroscopy, *Appl. Phys. Lett.* **101**, 022105 (2012).
- [51] S. Hwan Lee, D. Lee, W. Sik Hwang, E. Hwang, D. Jena, and W. Jong Yoo, High-performance photocurrent generation from two-dimensional WS₂ field-effect transistors, *Appl. Phys. Lett.* **104**, 193113 (2014).
- [52] B. Zhu, X. Chen, and X. Cui, Exciton binding energy of monolayer WS₂, *Sci. Rep.* **5**, 9218 (2015).
- [53] T. Ahmed, S. Islam, T. Paul, N. Hariharan, S. Elizabeth, and A. Ghosh, A generic method to control hysteresis and memory effect in Van der Waals hybrids, *Mat. Res. Exp.* **7**, 014004 (2020).
- [54] S. Ghatak, A. N. Pal, and A. Ghosh, Nature of electronic states in atomically thin MoS₂ field-effect transistors, *ACS Nano* **5**, 7707 (2011).